Three-dimensional real-time tracking of nanoparticles at an oil-water interface

Kan Du[†,‡] J. Alexander Liddle [*,†] and *Andrew J. Berglund* [*,†]

† Center for Nanoscale Science and Technology, National Institute of Standards and Technology, Gaithersburg, MD 20899

‡ Maryland Nanocenter, University of Maryland, College Park, MD 20742

* email: liddle@nist.gov; ajberglund@gmail.com

Abstract

Single-particle tracking with real-time feedback control can be used to study three-dimensional nanoparticle transport dynamics. We apply the method to study the behavior of adsorbed nanoparticles at a silicone oil-water interface in a microemulsion system over a range of particles sizes from 24 nm to 2 000 nm. The diffusion coefficient of large particles (> 200 nm) scales inversely with particle size, while smaller particles exhibit an unexpected increase in drag force at the interface. The technique can be applied in the future to study three-dimensional dynamics in a range of systems, including complex fluids, gels, biological cells and geological media.

1. Introduction

The dynamics of colloidal nanoparticles in complex media are of considerable interest in fields ranging from cell biology to oil exploration and recovery .[1-14] Given the three-dimensional nature of such media, it is important to be able to follow the nanoparticles in full 3D space in order to capture all the essential aspects of their behavior and so probe the underlying physics. In this work, we apply a real-time, 3D tracking system to determine the diffusion coefficients of nanoparticles absorbed at the oil-water interfaces of oil droplets in a micro-emulsion. Nanoparticles absorbed at an interface are

confined and can move only laterally along the interfaces because of the large adsorption energy.[15,16]

The interfacial dynamics of adsorbed nanoparticles provide a mechanism for probing such interfaces and are also relevant to understanding such phenomena as the formation of and stability of Pickering emulsions and particle assembly at interfaces. However, several open questions remain regarding the basic physics of interfacial nanoparticle transport, primarily because of the lack of tools available for probing dynamics *in situ*. Several experimental methods, such as laser scanning confocal microscopy, optical microscopy and fluorescence photobleaching, have been applied to investigate the interfacial dynamics of colloidal particles.[17-25] These methods have limits in particle size, spatial resolution, temporal resolution, and typically require special sample preparations to create flat interfaces suitable for conventional microscopy. Confocal microscopy can effectively measure the three-dimensional (3D) positions of multiple particles by acquiring stacks of images in the z direction, but the stack acquisition rate (on the order of 1 Hz to 10 Hz) is relatively slow for tracking fast moving nanoparticles in 3D.[26-29] Recent advances in optical microscopy have enabled 3D tracking of multiple particles simultaneously,[30-33] but their operation is constrained to within a distance on the order of the depth of focus from the microscope's focal plane, and therefore well-controlled interfaces unavailable in real-world geometries such as gels, emulsions, or geological media must be used. Complementing and motivating the experimental studies, there are a large number of theoretical investigations on interfacial dynamics of colloidal particles.[34-38] Different analytical and numerical conclusions have been obtained under different assumptions. While several experimental measurements have been applied to verify or support the theoretical conclusions, there remains an important gap between experimental observations and theoretical explanation. One possible source of discrepancy is the use of homogeneous continuum approaches in theoretical investigations of interfacial dynamics, where heterogeneous fluidic or even atomic structure may become important at the nanoscale.[39] Furthermore, issues such as surface charge, heterogeneity of surface functionality ("patchiness"), three-phase line tensions, physical ageing of contact lines, size-dependent hydrophobicity, interface curvature and interface deformation are expected

to play crucial roles, again becoming increasingly important at the nanoscale.[40-48] It is critically important, therefore, to develop new, accurate methods for making experimental measurements of interfacial nanoparticle dynamics in realistic systems.

In this paper we use a 3D real-time feedback tracking apparatus to investigate interfacial dynamics of fluorescent polystyrene nanoparticles in oil-in-water emulsions by monitoring the *in situ* motion of individual nanoparticles at the oil-water interfaces of droplets, over a wide range of nanoparticle sizes in a true 3D geometry. The 3D positions of nanoparticles diffusing at the surfaces of oil droplets are tracked with high spatial (≈50 nm) and temporal (≈5 ms) resolution. Diffusion coefficients (D) of nanoparticles with diameters ranging from 24 nm to 2 000 nm, have been measured both at interfaces and in water. For freely diffusing particles in water, measured D scale linearly with the inverse of particle radius (R^{-1}) and agree well with theoretical values estimated from the Stokes-Einstein equation. For particles adsorbed at interfaces, diffusion coefficients are reduced because of the high viscosity of the oil. Surprisingly, measured D do not scale linearly with R^{-1} and small particles (diameter < 200 nm) diffuse relative slowly. The measurements indicate that the drag coefficient (normalized to the particle radius R) increases as the size of particles decreases. The standard drag coefficient equation accounts for the interaction of the absorbed particle with the liquids on both sides of the interface using a contact angle-dependent function. However, we find that this equation can only be fit to the data by allowing the contact angle to vary with particle size. Using this assumption, we estimate that the contact angle of particles at interfaces decreases from 0.9 π to 0.5 π as the particle size decreases from 2 000 nm to 24 nm. We discuss several physical phenomena that might lead to such behavior, including variation in surface functionality, charge-induced interface deformation, interface curvature and three-phase line tension. Based on the data, we propose that three-phase line tension is the dominant effect. Our results demonstrate the capability of real-time 3D tracking for investigating *in situ* dynamics of interfacial nanoparticles in 3D geometries, with high spatial and temporal resolution. The method opens the possibility for studying transport phenomena in other complex, intrinsically three-dimensional materials,

including complex fluids, gels, biological cells and geological media.

2. Experimental Section

(i) 3D real-time feedback tracking apparatus

Building on recent advancements in real-time feedback control of diffusing particles,[49-54] we have developed an apparatus to perform 3D tracking of individual fluorescent nanoparticles at oil-water interfaces. Figure 1(a) shows the experimental design. The basic idea is that a focused excitation laser is scanned in a small (sub-micron) periodic pattern, while fluorescence photons are collected and demodulated in real-time to derive a feedback signal suitable for closed-loop tracking with a 3D piezo electric stage. Our design closely follows that of reference.[50] A 532 nm laser beam is first deflected along the x-axis at frequency $f_{xy} = 312.5$ kHz by an acousto-optic deflector (AOD 1), then split into two beams by a polarizing beamsplitter (PBS). Both beams are then deflected along the y-axis at the same frequency f_{xy} by AODs 2 & 3. In order to deflect the beams in a circular pattern, the y-axis deflections have 90 $^{\text{o}}$ phase shift from the x-axis deflection (this phase shift value is subsequently adjusted to correct for small variations in beam alignment and resulting acoustic propagation times). By attenuating the radio frequency (r.f) drive signals into the y-axis AODs, the optical powers of beams 1 and 2 are alternately turned on or off at frequency $f_z = f_{xy}/2 = 156.25$ kHz to create intensity variation along the z-axis. The beams pass through lens pairs, allowing independent adjustment of their focal planes in the sample before being combined by another PBS. Finally, the beams are focused by a microscope objective (63x/NA 1.2 water immersion) into a liquid sample. The result is an alternating cycle of circular scans above and below the (detection) focal plane. Nanoparticle fluorescence is collected by the objective lens, separated from the excitation light by a dichroic filter, and measured by a single-photon counting Si avalanche photodiode. As the block diagram (Figure 1(b)) shows, the fluorescence signal is demodulated on a field-programmable gate array (FPGA) programmed in LabView.[55-57] The error signals are fed back to a three-axis piezoelectric sample stage (75 μm travel in

4

xy, 50 μm travel in z) to move the sample and lock the nanoparticle in the focus of the objective lens. Although the feedback control loop operates in quasi-continuous time (discretized only by the FPGA clock signal at 40 MHz =1/25 ns), data is recorded at a lower rate for convenience. The stage positions along x, y and z axis and the fluorescence intensity are recorded every millisecond. The overall bandwidth of the feedback system is several hundred Hertz, limited by the mechanical response of the piezoelectric nanopositioning stage.

(ii) Sample preparation

We use silicone oil (Sigma Aldrich, product # 146153) with density of 0.97 g/cm^3 and viscosity of 100 mPa s at 25 °C (measured by a viscometer). The nanoparticles (Invitrogen, product # F8887) are carboxylate-modified polystyrene spherical beads with nominal diameters of 24 nm, 100 nm, 200 nm, 490 nm, 1100 nm, and 2000 nm. According to the manufacturer, the coefficient of variation (standard deviation/mean size) of bead diameter is 20 % for 24-nm beads and 5 % for 100 nm and larger beads. We confirmed the size of the beads to be consistent with the manufacturer values by scanning electron microscopy (SEM). The polystyrene beads are labeled with red fluorescent dye, which has an emission peak at 650 nm. The beads are negatively charged due to their carboxylate modification. Prior to use, the beads are cleaned by performing several cycles of centrifugation and washing to remove azide preservative and residual surfactant.

Oil-in-water emulsions are simply prepared by adding 30 μL silicone oil into 200 μL aqueous suspension of nanoparticles then shaking the mixture by hand for a few minutes. The obtained oil droplets have diameters ranging from ten to several hundred microns. To ensure that we observe a single, isolated particle, the bulk concentration of the initial nanoparticle suspension is reduced such that we observe on average less than 1 particle per oil droplet. After preparation, a small volume (20 μL) of the resulting emulsion is sealed in a sample cell made of two glass coverslips with approximately 100 μm depth. For 3D nanoparticle tracking experiments, we only choose the oil droplets stuck to the lower

glass surface, as Figure 2 shows, to eliminate the diffusion of free oil droplets.

3. Results and Discussion

Using our 3D tracking apparatus, we measured diffusion dynamics of polystyrene particles with diameter from 24 nm to 2 000 nm at oil-water interfaces. Figure 3 (a-c) shows a typical measurement result from a 3D tracking experiment. A 200 nm-diameter polystyrene particle is adsorbed and diffusing at the surface of a silicone oil droplet in water. The particle is tracked for over 300 s, until it reaches the travel limit of the piezoelectric sample stage (at which point the controller resets and the stage is moved back to its center position). A 3D trajectory plot and projections onto xy, xz and yz planes clearly reveal the spherical profile of the oil droplet with a diameter around 10 μm.

The diffusion coefficient (D) of a particle is estimated from the mean-square displacement using $D = \frac{\Delta r^2}{2d\Delta t} = \frac{1}{d}(D_x + D_y + D_z)$, where $\Delta r^2 = \Delta x^2 + \Delta y^2 + \Delta z^2$ is the change in the particle's (three-dimensional) position in time Δt (See Figure 4).[58] For example, $D_x = \frac{\Delta x^2}{2\Delta t}$. For free particles moving in 3D we take $d = 3$ while for interfacial particles, the surface diffusion coefficient is found by taking $d = 2$ to account for the reduced dimensionality of the surface.[59] For a particle freely diffusing in water, the diffusion coefficient along x, y and z is expected to be isotropic, $D_x = D_y = D_z$, due to the homogeneous environment. One of our control experiments on a freely diffusing particle confirms D_x, D_y and D_z have the same values for a 200 nm particle in water. Figure 4 (a) shows the 3D trajectory of the particle. Figure 4 (c) shows the calculated mean square displacement (MSD) (upper) and diffusion coefficient vs delay time (lower) plots. The measured diffusion coefficient $D = (D_x + D_y + D_z)/3 = (2.1 \pm 0.04)$ μm^2/s , which is good agreement with the theoretical value (2.2 ± 0.1) μm^2/s estimated from the Stokes-Einstein equation (uncertainties are 1 standard deviation; the uncertainty in the theoretical estimate reflects the uncertainty in the particle size). In the lower plot of Figure 4(c), the diffusion coefficient appears smaller than the true value at short times (< 5 ms), because the tracking apparatus

has a finite response bandwidth. Re-plotting the data in this format aids the experimentalist in determining when the feedback loop is under- or overdamped and is analogous to the determination of the step response of a control system. An estimate of D in this type of plot can be found from the flat (constant) portion of the curves. We estimate the error in the observed diffusion coefficient through repeated measurements – typically estimating D on each 1-second interval of a trajectory. Quoted errors are one standard deviation of the measured Ds. For an adsorbed particle at oil-water interfaces, D_x, D_y and D_z depend on the angles between the axes and interfaces because of inhomogeneous constraints along x, y and z axes. Figure 4 (b) is a 20 s part of the trajectory of a particle absorbed at an oil/water interface shown in Figure 3 (b). The calculated diffusion coefficients are, as Figure 4 (d) shows, $D_x = (0.04 \pm 0.004)$ μm^2/s, $D_y = (0.12 \pm 0.008)$ μm^2/s, $D_z = (0.08 \pm 0.006)$ μm^2/s. As the particle moves on the surface of the oil droplet, the individual values of D_x, D_y and D_z change as the particle explores the different local orientations of the interface. However, the surface diffusion coefficient $D = (D_x + D_y + D_z)/2 = (0.12 \pm 0.006)$μm^2/s remains constant, within experimental error.

Figure 5(a) shows the measured D of polystyrene particles with diameters ranging from 24 nm to 2 000 nm. For freely diffusing particles in water (diamonds), the measured D agrees with the theoretical value estimated from the Stokes-Einstein equation: $D_w = kT/(6\pi\eta_w R)$. Here, k is Boltzmann constant, T is temperature, $\eta_w = 1.0$ mPa s is the viscosity of water at room temperature, R is the particle radius. The measurements on freely diffusing particles demonstrate the accuracy and reliability of the 3D tracking apparatus over a wide range of particle sizes and diffusion coefficients. The diffusion coefficient of particles absorbed at an oil-water interface would be expected to fall in between those for diffusion in water and oil, with the value depending on the contact angle at the three-phase boundary. However, the measured values of D (circles) approach the value expected for diffusion in oil at small particle sizes. We also note that the spread in measured diffusion coefficients is significantly larger than

the measurement error, or that expected from particle size variations, for the particles absorbed at the oil/water interface – in contrast to the results for the freely-diffusing particles.

One possible explanation for non-linear dependence of D on R^{-1} is the charge-induced deformation of the oil-water interface around the adsorbed particles.[45] To investigate these electrocapillary effects, we performed control experiments, in which the pH value is decreased to 4, the isoelectric point of the carboxylate group, to neutralize the charge on polystyrene particles. However, as Figure 5(a) shows, nearly identical results are measured for charged and neutralized nanoparticles, suggesting that the charge-induced deformation model is not an explanation for the increased drag coefficients. In the figure, data at pH=4 (triangle) is shifted to the right to avoid overlapping plots.

Curvature of the interface may also be expected to play a role in interfacial diffusion, but here the radius of curvature of the droplet is at least an order of magnitude larger than the radius of curvature of the particle. We measured D of polystyrene particles (24 nm, 200 nm, 1 100 nm) at the surfaces of oil droplets with different diameters. As the Figure 6 shows, the measured D is independent of oil droplet diameter, demonstrating that curvature effects on interfacial dynamics are negligible for our measurements on oil droplets.

Another possibility is a variation in contact angle with particle size. We can estimate what contact angle would be necessary to explain the observed diffusion coefficients using a modified Stokes-Einstein equation, $D = \frac{kT}{f\eta_o R}$, to describe the Brownian diffusion of spherical particles at locally flat liquid-liquid interfaces.[37,38] Here, f is a drag coefficient, which is a complicated nonlinear function of the contact angle θ and the viscosities of water η_w and oil η_o. In our experiments, $\eta_w/\eta_o \approx 0.01$, so that the nonlinear function can be simplified (taking $\eta_w/\eta_o \to 0$) : $f = 6\pi \left(\tanh \frac{32(1+\cos\theta)}{9\pi^2}\right)^{\frac{1}{2}}$.[37] Thus, the contact angle of adsorbed nanoparticles at oil-water interfaces under the assumption of a locally flat interface can be calculated from the measured D with the following equation:

$\cos\theta = \frac{9\pi^2}{32}\text{arctanh}(\frac{D_o}{D})^2 - 1$. Here the diffusion coefficient of particles in oil (D_o) is calculated from the Stokes-Einstein equation. As Figure 5(b) shows, the calculated θ decreases from 0.9 π to 0.5 π as the diameter of particle decreases from 2 000 nm to 24 nm. θ decreases rapidly for particles with diameter less than 200 nm, deviating strongly from the expected R^{-1} scaling.

The decreasing contact angle might occur as result of a variation in surface coverage of functional groups on the polystyrene surface. However, it is not clear why such a variation would be monotonic with particle size. "Patchiness" or heterogeneity in coverage could also be expected to give increasing variability at small sizes, due to resulting variations in contact angle or local deformation of the interface; however, one expects these effects to increase the variability but not necessarily change the mean value of the drag force. Effects associated with particle surface heterogeneity may explain the increased spread in the diffusion coefficients measured for the absorbed particles. In order to study the variability in surface functionality, we performed Zeta potential measurements with two different methods (electro-osmotic flow and dynamic light scattering), but results were inconclusive over the large range of particle sizes studied here. This is indicative of a significant and general difficulty in characterizing the surface functionality of individual nanoparticles.[41,42]

Another possibility that might explain the changing contact angle with particle size is the three-phase (particle, oil and water) line tension τ, which has been observed to be positive or negative in experimental and theoretical studies alike.[43,44] Line tension can cause changes in the contact angle of nanoparticles at interfaces, and becomes important for smaller particles as the perimeter-to-surface-area ratio increases. To test whether line tension explains our observations, we fit our data using a modified Young-Dupre equation:[43] $\cos\theta = (\cos\theta_0)(1 - \frac{\tau}{R\gamma_{ow}Sin\theta})^{-1}$ where, $\theta_0 = (\gamma_{pw} - \gamma_{po})/\gamma_{ow}$ is the contact angle when $\tau = 0$. Here, $\gamma_{ow} = 50$ mN/m.[60] $\theta_0 = 0.9$ π is the calculated contact angle of 2 000 nm polystyrene particles, which experience a negligible line tension effect. This value of θ_0 is consistent with that estimated from an optical image.[16] As figure 5(c) shows, the line tension model shows

qualitatively similar behavior to the measured values if the line tension is negative. Negative line tension would pull the particles towards the interface and consequently increases the immersion depth into the oil. In that case, small particles would diffuse more slowly because of increased drag coefficients. The line tension model cannot exactly reproduce the measured data, which indicates the existence of other effects.

4. Conclusions

We have applied real-time feedback control tracking of single fluorescent particles to study the transport of adsorbed nanoparticles at a silicone oil-water interface over two orders of magnitude in particle size. Our results show anomalous behavior for small particles (< 200 nm), which may be partially explained by systematic variation in surface functionality or negative line tension effects but do not appear to arise from electrocapillary (charge) effects. The technique is robust and can in the future be applied in studying nanoparticles in crowded interfacial assemblies and other three-dimensional systems, such as biological cells, complex fluids, or geological media.
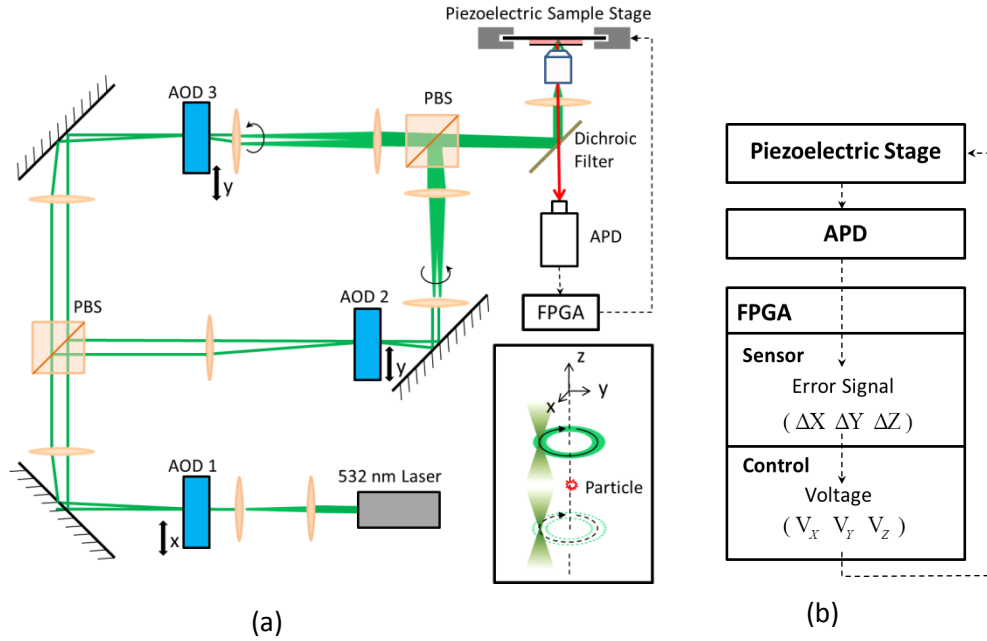
Figure 1(a) Schematic diagram of the experimental apparatus for tracking freely diffusing fluorescent nanoparticles in three dimensions. Inset shows that two focused lasers scan in a two-circle pattern in the focus of a microscope objective lens; the circular scans have 500 nm radius, while the difference in z positions is 1.5 μm. A fluorescent nanoparticle is locked in the center of the pattern. AOD: acoustic optical deflector; PBS: polarized beam splitter; APD: avalanche photodiode; FPGA: field programmable gated array. (b) Block diagram of the particle tracking system.

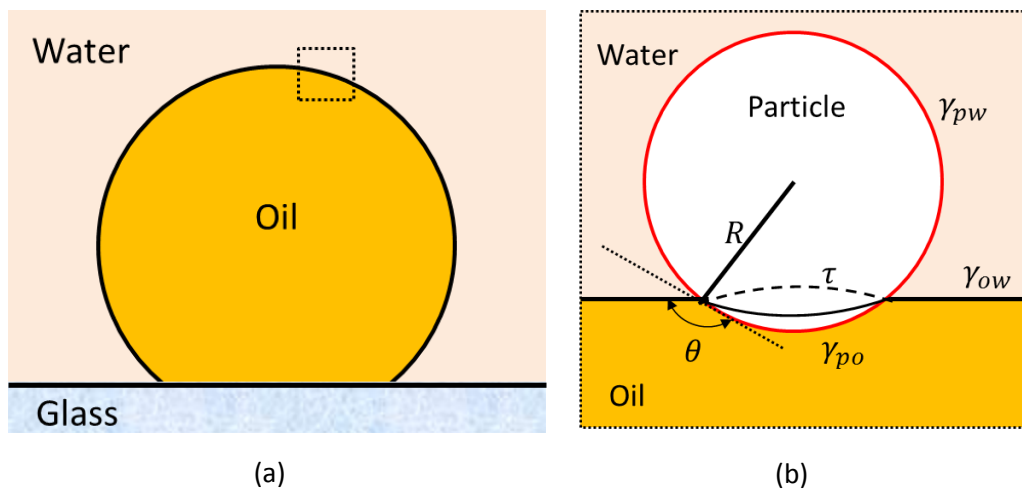(a)   (b)

Figure 2. (a) Schematic diagram of a sample: a silicone oil droplet stuck to surface of glass coverslip is immersed in aqueous suspension of polystyrene nanoparticles. (b) Inset shows an adsorbed polystyrene nanoparticle diffusing at surface of the oil droplet.
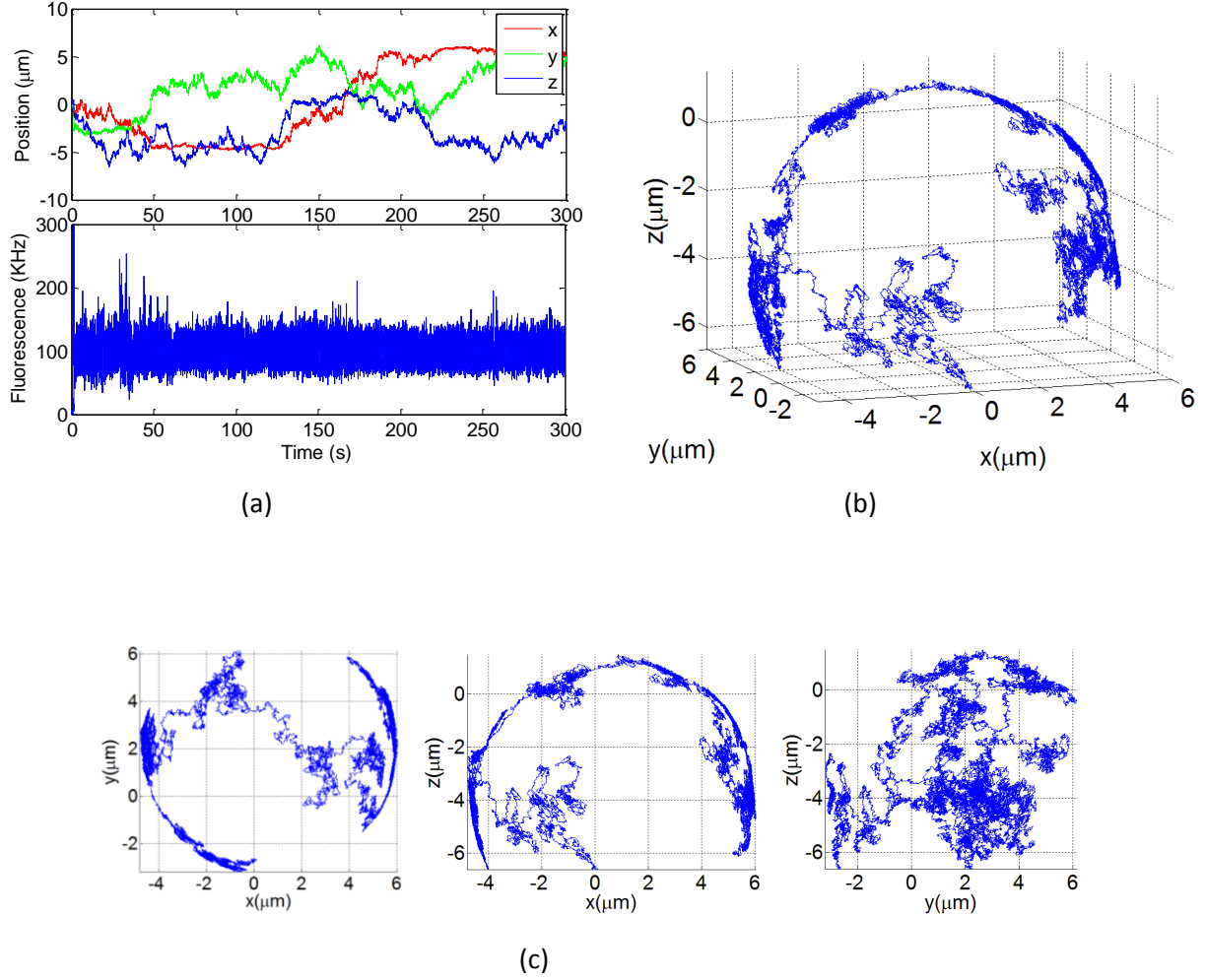
(a)

(b)

(c)

Figure 3. (a) 3D tracking of a 200 nm diameter polystyrene particle diffusing at the surface of a silicone oil droplet in water. Top: x, y, z positions of tracking stage. Bottom: fluorescence intensity. (b) 3D trajectory shows the profile of oil droplet. (c) Projections of the trajectory onto xy, xz and yz plane.
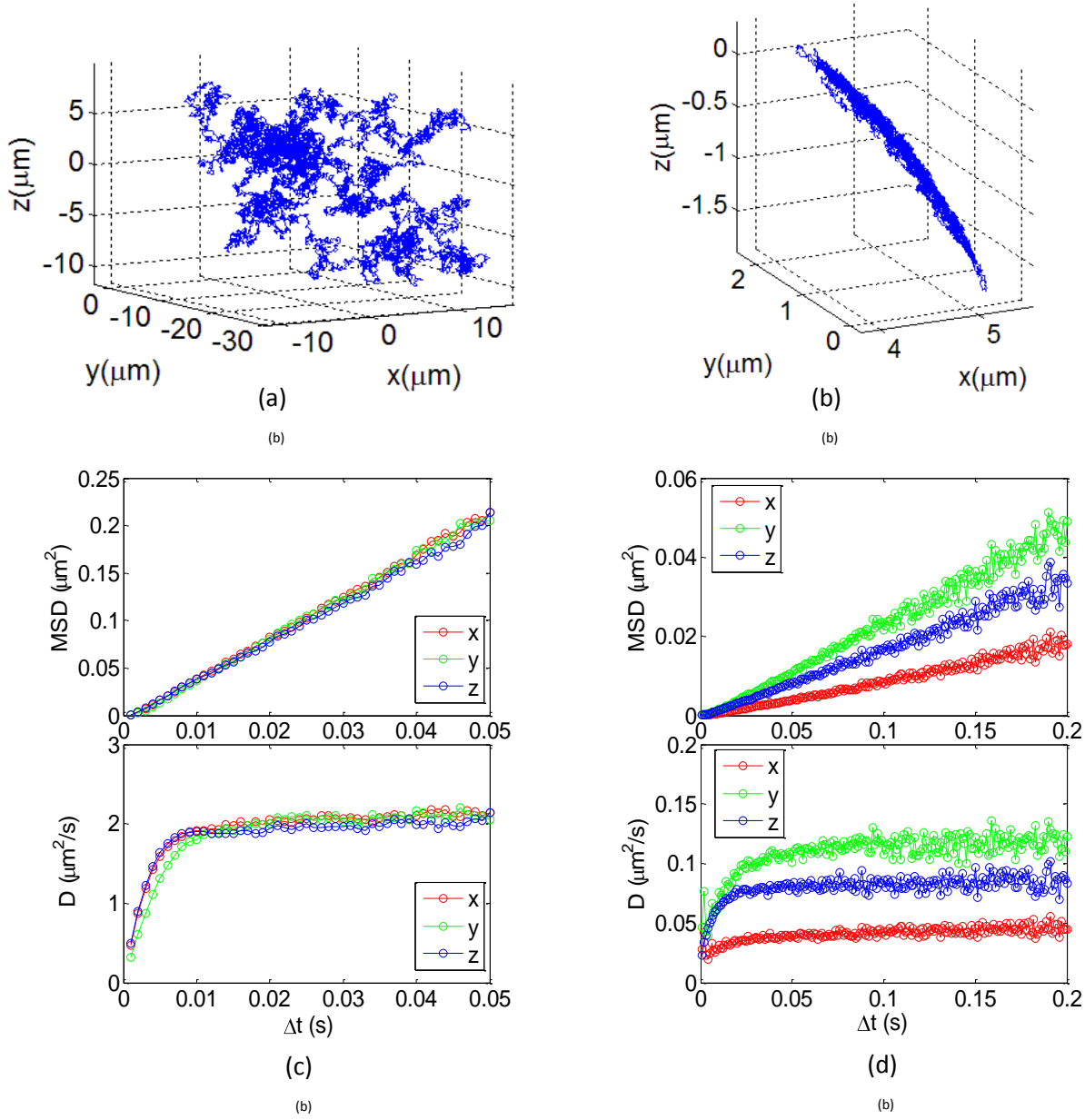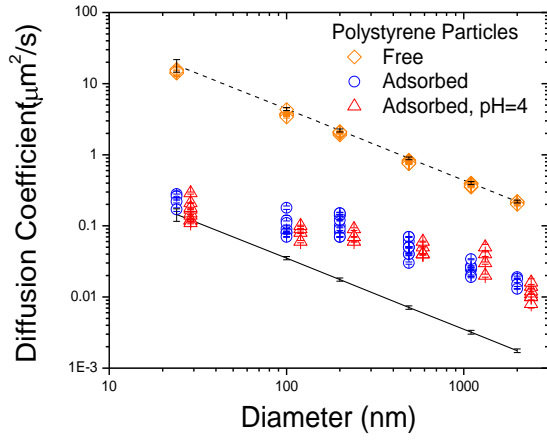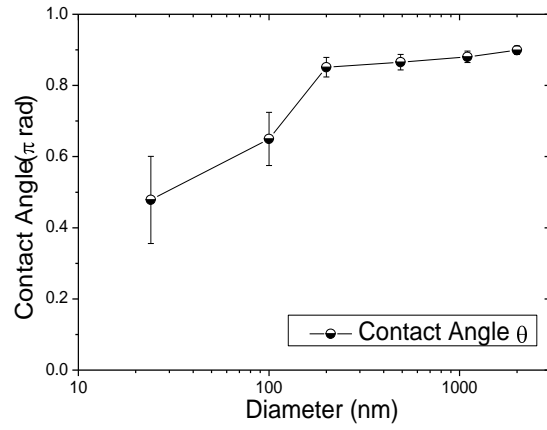
Figure 4. Three dimensional trajectories of individual polystyrene nanoparticles (200 nm in diameter) diffusing (a) freely in water and (b) at oil-water interface. (c) Freely diffusing nanoparticle has identical diffusion coefficient in x, y and z directions. Upper: mean square displacement (MSD) vs delay time plot. Lower: diffusion coefficient vs delay time plot. (d) Adsorbed nanoparticle has different diffusion coefficient in x, y and z directions due to the constraint of oil-water interface. The MSD plot is simply given by $\mathrm{MSD} = \frac{1}{E(N/n)} \sum_{i=1}^{E(N/n)} (\vec{r}_{i+n} - \vec{r}_i)^2)$, n= 1, …, N-1, where the delay time, $\Delta t = n \, \delta t$ (δt is the time interval between data points) and $D = \mathrm{MSD}/2d\Delta t$. The MSD is known to exhibit systematic errors in camera-based measurements, when tracking errors and camera integration time is ignored.[61,62] The effect of localization noise and tracking errors in the feedback controlled case are analyzed in previous work,[63] where it is found that the MSD asymptotically approaches the true diffusion coefficient. Analysis of MSD curves also indicates three-dimensional tracking (localization) errors of approximately 100 nm for freely diffusing nanoparticles and 50 nm for adsorbed nanoparticles.
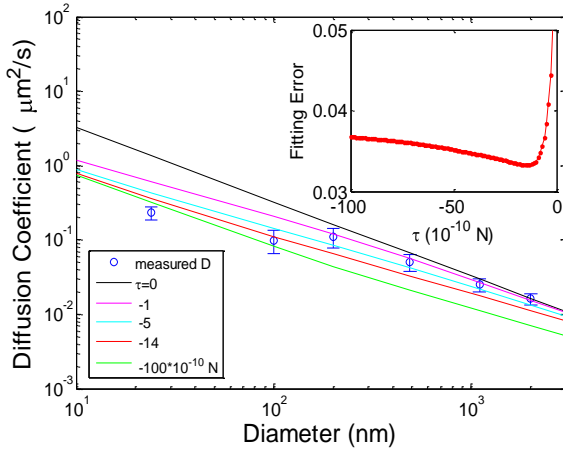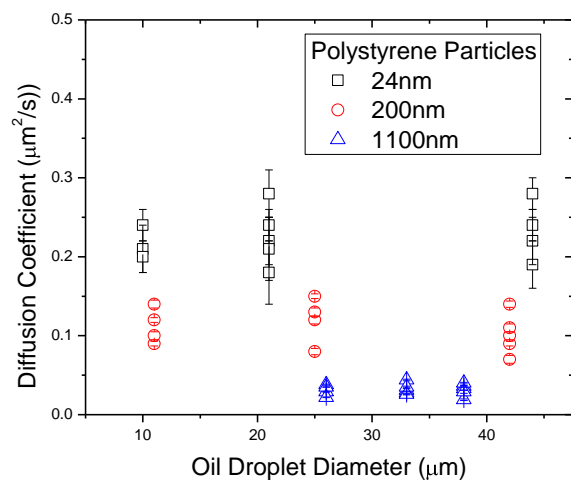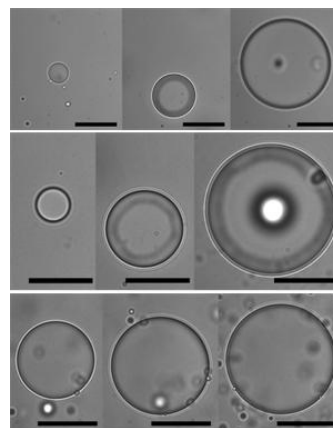
(a)

(b)

(c)

Figure 5. (a) Measured D of polystyrene particles with diameters from 24 nm to 2 000 nm. For freely diffusing particles in water, the measured D (diamonds) is consistent with theoretical value estimated from the Stokes-Einstein equation (dotted line), i.e. D is proportional to R^{-1}. Error bars are marked on the theoretical lines to take account of the uncertainty in particle size. For particles absorbed at an oil-water interface, the measured D (circles) does not linearly scale with R^{-1}. The measured values of D have more than an order of magnitude deviation from the values expected for the smallest particle sizes, tending towards that expected for diffusion in oil (solid line). The same result is observed when the charge on the particles is neutralized by changing the pH value to 4. The data (triangle) are shifted to right to avoid overlapping plots. (b) The calculated contact angle, θ, decreases from 0.9 π to 0.5 π as the diameter of particle decreases from 2000 nm to 24 nm. (c) Fit to measured D values obtained with line tension model. From top to bottom, $\tau = (0, -1, -5, -14, -100) \times 10^{-10} N$. The inset shows the fitting error has a minimum at $\tau = -14 \times 10^{-10} N$.

Figure 6 (a) Diffusion coefficient (D) of polystyrene particles (24 nm, 200 nm, 1 100 nm in diameter) at surfaces of oil droplets with different diameters. The value of D is independent of oil drop diameter, demonstrating that curvature effects on interfacial dynamics are negligible for our measurements. (b) Optical microscope images of oil droplets with different diameter. Top: 24 nm polystyrene particles. Middle: 200 nm. Bottom: 1 100 nm. The scale bars are 20 μm.

References

(1)   Saxton, M. J.; Jacobson, K. SINGLE-PARTICLE TRACKING: Applications to Membrane Dynamics. *Annu. Rev. Biophys. Biomol. Struct.* **1997**, *26*, 373–399.

(2)   Sako, Y.; Minoghchi, S.; Yanagida, T. Single-molecule imaging of EGFR signalling on the surface of living cells. *Nat. Cell Biol.* **2000**, *2*, 168–172.

(3)   Seisenberger, G.; Ried, M. U.; Endress, T.; Büning, H.; Hallek, M.; Bräuchle, C. Real-time single-molecule imaging of the infection pathway of an adeno-associated virus. *Science* **2001**, *294*, 1929.

(4)   Forstner, M. B.; Martin, D. S.; Navar, A. M.; Käs, J. A. Simultaneous Single-Particle Tracking and Visualization of Domain Structure on Lipid Monolayers. *Langmuir* **2003**, *19*, 4876–4879.

(5)   Xie, X. S.; Yu, J.; Yang, W. Y. Living Cells as Test Tubes . *Science* **2006**, *312*, 228–230.

(6)   Moerner, W. E. New Directions in Single-Molecule Imaging and Analysis. *Proc. Natl. Acad. Sci. U. S. A.* **2007**, *104*, 12596–12602.

(7)   Jaqaman, K.; Loerke, D.; Mettlen, M.; Kuwata, H.; Grinstein, S.; Schmid, S. L.; Danuser, G. Robust single-particle tracking in live-cell time-lapse sequences, *Nat. Methods* **2008**, *5*, 695–702.

(8)   Sahl, S. J.; Leutenegger, M.; Hilbert, M.; Hell, S. W.; Eggeling, C. Fast Molecular Tracking Maps Nanoscale Dynamics of Plasma Membrane Lipids. *Proc. Natl. Acad. Sci. U. S. A.* **2010**, *107*, 6829–6834.

(9)   Sriram, I.; Walder, R.; Schwartz, D. K. Stokes–Einstein and desorption-mediated diffusion of protein molecules at the oil–water interface. *Soft Matter* **2012**.

(10)   Sahimi, M. *Flow and transport in porous media and fractured rock: From classical methods to modern approaches*; Wiley-VCH, **1995**.

(11)   Kandhai, D.; Hlushkou, D.; Hoekstra, A. G.; Sloot, P. M. A.; Van As, H.; Tallarek, U. Influence of Stagnant Zones on Transient and Asymptotic Dispersion in Macroscopically Homogeneous Porous Media. *Phys. Rev. Lett.* **2002**, *88*, 234501.

(12)   Hassan, A. E.; Mohamed, M. M. On using particle tracking methods to simulate transport in single-continuum and dual continua porous media. *J. of Hydrol.* **2003**, *275*, 242–260.

(13)   Ortega, F.; Ritacco, H.; Rubio, R. G. Interfacial microrheology: Particle tracking and related techniques. *Current Opinion in Colloid & Interface Science* **2010**, *15*, 237–245.

(14)   Bijeljic, B.; Mostaghimi, P.; Blunt, M. J. Signature of Non-Fickian Solute Transport in Complex Heterogeneous Porous Media. *Phys. Rev. Lett.* **2011**, *107*, 204502.

(15)   Pieranski, P. Two-Dimensional Interfacial Colloidal Crystals. *Phys. Rev. Lett.* 1980, *45*, 569- 572.

(16)   Du, K.; Glogowski, E.; Emrick, T.; Russell, T. P.; Dinsmore, A. D. Adsorption Energy of Nano- and Microparticles at Liquid−liquid Interfaces. *Langmuir* **2010**, *26*, 12518-12522.

(17)   Vignati, E.; Piazza, R.; Lockhart, T. P. Pickering Emulsions: Interfacial Tension, Colloidal Layer Morphology, and Trapped-Particle Motion. *Langmuir* **2003**, *19*, 6650–6656.

(18)   Lin, Y.; Böker, A.; Skaff, H.; Cookson, D.; Dinsmore, A. D.; Emrick, T.; Russell, T. P. Nanoparticle Assembly at Fluid Interfaces: Structure and Dynamics. *Langmuir* **2005**, *21*, 191-194.

(19)   Peng, Y.; Chen, W.; FISCHER, T.; Weitz, D.; Tong, P. Short-Time Self-Diffusion of Nearly Hard Spheres at an Oil-Water Interface. *J. Fluid Mech.* **2009**, *618*, 243–261.

(20)   Tarimala, S.; Ranabothu, S. R.; Vernetti, J. P.; Dai, L. L. Mobility and In Situ Aggregation of Charged Microparticles at Oil-Water Interfaces. *Langmuir* **2004**, *20*, 5171–5173.

(21)   Dai, L. L.; Tarimala, S.; Wu, C.; Guttula, S.; Wu, J. The Structure and Dynamics of Microparticles at Pickering Emulsion Interfaces. *Scanning* **2008**, *30*, 87–95.

(22)   Lee, M. H.; Cardinali, S. P.; Reich, D. H.; Stebe, K. J.; Leheny, R. L. Brownian Dynamics of Colloidal Probes During Protein-Layer Formation at An Oil–Water Interface. *Soft Matter* **2011**, *7*, 7635.

(23)   Dhar, P.; Prasad, V.; Weeks, E. R.; Bohlein, T.; Fischer, T. M. Immersion of Charged Nanoparticles in a Salt Solution/Air Interface. *J. Phys. Chem. B* **2008**, *112*, 9565–9567.

(24)   Schwartz, H.; Harel, Y.; Efrima, S. Surface Behavior and Buckling of Silver Interfacial Colloid Films. *Langmuir* **2001**, *17*, 3884-3892.

(25)   Stocco, A.; Mokhtari, T.; Haseloff, G.; Erbe, A.; Sigel, R. Evanescent-wave dynamic light scattering at an oil-water interface: Diffusion of interface-adsorbed colloids. *Phys. Rev. E* **2011**, *83*, 011601.

(26)   Nakano, A. Spinning-disk Confocal Microscopy — A Cutting-Edge Tool for Imaging of Membrane Traffic. *Cell Structure and Function* **2002**, *27*, 349–355.

(27)   Dinsmore, A. D.; Weeks, E. R.; Prasad, V.; Levitt, A. C.; Weitz, D. A. Three-dimensional confocal microscopy of colloids. *Applied Optics* **2001**, *40*, 4152–4159.

(28)   Dupont, A.; Lamb, D. C. Nanoscale three-dimensional single particle tracking. *Nanoscale* **2011**, *3*, 4532.

(29)   Shen, Z.; Andersson, S. B. 3-D tracking of fluorescent nanoparticles in a confocal microscope. *50th IEEE Conference on Decision and Control and European Control Conference* **2011**.

(30)   Pavani, S. R. P.; Thompson, M. A.; Biteen, J. S.; Lord, S. J.; Liu, N.; Twieg, R. J.; Piestun, R.; Moerner, W. E. Three-Dimensional, Single-Molecule Fluorescence Imaging Beyond the Diffraction Limit by Using a Double-Helix Point Spread Function. *Proc. Natl. Acad. Sci. U. S. A.***2009**, *106*, 2995–2999.

(31)   Thompson, M. A.; Lew, M. D.; Badieirostami, M.; Moerner, W. E. Localizing and Tracking Single Nanoscale Emitters in Three Dimensions with High Spatiotemporal Resolution Using a Double-Helix Point Spread Function. *Nano Lett.* **2009**, *10*, 211–218.

(32)   Kao, H. P.; Verkman, A. S. Tracking of single fluorescent particles in three dimensions: use of cylindrical optics to encode particle position. *Biophys. J.* **1994**, *67*, 1291–1300. Holtzer, L.; Meckel, T.; Schmidt, T. Nanometric three-dimensional tracking of individual quantum dots in cells. *Appl. Phys. Lett.* **2007**, *90*, 053902 –053902–3. Huang, B.; Wang, W.; Bates, M.; Zhuang, X. Three-Dimensional Super-Resolution Imaging by Stochastic Optical Reconstruction Microscopy. *Science* **2008**, *319*, 810–813.

(33)   Juette, M. F.; Gould, T. J.; Lessard, M. D.; Mlodzianoski, M. J.; Nagpure, B. S.; Bennett, B. T.; Hess, S. T.; Bewersdorf, J. Three-dimensional sub-100 nm resolution fluorescence microscopy of thick samples. *Nature Methods* **2008**, *5*, 527–529.

(34)   Saffman, P. G.; Delbrück, M. Brownian Motion in Biological Membranes. *Proc. Natl. Acad. Sci. U. S. A.* **1975**, *72*, 3111 -3113.

(35)   Radoev, B.; Nedyalkov, M.; Dyakovich, V. Brownian Motion at Liquid-Gas Interfaces. 1. Diffusion Coefficients of Macroparticles at Pure Interfaces. *Langmuir* **1992**, *8*, 2962–2965.

(36)   Danov, K.; Aust, R.; Durst, F.; Lange, U. Influence of the Surface Viscosity on the Hydrodynamic Resistance and Surface Diffusivity of a Large Brownian Particle. *J. Colloid Interface Sci.* **1995**, *175*, 36–45.

(37)   Fischer, T. M.; Dhar, P.; Heinig, P. The Viscous Drag of Spheres and Filaments Moving in Membranes or Monolayers. *J. Fluid Mech.* **2006**, *558*, 451–475.

(38)   Brenner, H.; Leal, L. A Micromechanical Derivation of Fick's Law for Interfacial Diffusion of Surfactant Molecules. *J. Colloid Interface Sci.***1978**, *65*, 191–209.

(39)   Cheung, D. Molecular Simulation of Nanoparticle Diffusion at Fluid Interfaces. *Chem. Phys. Lett.* **2010**, *495*, 55–59.

(40)   Song, Y.; Luo, M.; Dai, L. L. Understanding Nanoparticle Diffusion and Exploring Interfacial Nanorheology using Molecular Dynamics Simulations. Langmuir 2009, 26, 5-9.

(41)   Sayes, C. M.; Warheit, D. B. Characterization of Nanomaterials for Toxicity Assessment. Wiley Interdiscip. Rev.: Nanomed. Nanobiotechnol. 2009, 1, 660–670.

(42)   Doane, T. L.; Chuang, C.-H.; Hill, R. J.; Burda, C. Nanoparticle ζ –Potentials. Acc. Chem. Res. 2011, 45, 317–326.

(43)   Bresme, F.; Oettel, M. Nanoparticles at Fluid Interfaces. J. Phys.: Condens. Matter 2007, 19, 413101.

(44)   Amirfazli, A.; Neumann, A. W. Status of the Three-Phase Line Tension: A Review. Adv. Colloid Interface Sci. 2004, 110, 121-141.

(45)   Nikolaides, M.; Bausch, A.; Hsu, M.; Dinsmore, A.; Brenner, M.; Gay, C.; Weitz, D.; Electric-Field-Induced Capillary Attraction Between Like-Charged Particles at Liquid Interfaces. Nature 2002, 420, 299–301.

(46)   Kaz, D. M.; McGorty, R.; Mani, M.; Brenner, M. P.; Manoharan, V. N. Physical Ageing of the Contact Line on Colloidal Particles at Liquid Interfaces. Nat. Mater. 2011, 11, 138–142.

(47)   Chiu, C.-cheng; Moore, P. B.; Shinoda, W.; Nielsen, S. O. Size-Dependent Hydrophobic to Hydrophilic Transition for Nanoparticles: A Molecular Dynamics Study. J. Chem. Phys. 2009, 131, 244706-244706-8.

(48)   Thijssen, J. H. J.; Schofield, A. B.; Clegg, P. S. How Do (Fluorescent) Surfactants Affect Particle-Stabilized Emulsions? Soft Matter 2011, 7, 7965–7968.

(49)   McHale, K.; Mabuchi, H. Precise Characterization of the Conformation Fluctuations of Freely Diffusing DNA: Beyond Rouse and Zimm. J. Am. Chem. Soc. 2009, 131, 17901-17907.

(50)   McHale, K.; Berglund, A. J.; Mabuchi, H. Quantum Dot Photon Statistics Measured by Three-Dimensional Particle Tracking. *Nano Lett.* **2007**, *7*, 3535–3539.

(51)   Levi, V.; Ruan, Q.; Kis-Petikova, K.; Gratton, E.; Scanning FCS, A Novel Method for Three-

Dimensional Particle Tracking. *Biochem. Soc. Trans.* **2003**, *31*, 997–1000.

(52)   Lessard, G. A.; Goodwin, P. M.; Werner, J. H. Three-Dimensional Tracking of Individual Quantum Dots. *Appl. Phys. Lett.* **2007**, *91*, 224106-224106-3.

(53)   Cang, H.; Wong, C. M.; Xu, C. S.; Rizvi, A. H.; Yang, H. Confocal Three Dimensional Tracking of a Single Nanoparticle with Concurrent Spectroscopic Readouts. *Appl. Phys. Lett.* **2006**, *88*, 223901-223901-3.

(54)   Juette, M. F.; Bewersdorf, J. Three-Dimensional Tracking of Single Fluorescent Particles with Submillisecond Temporal Resolution. *Nano Lett.* **2010**, *10*, 4657–4663.

(55)   Fields, A. P.; Cohen, A. E. Electrokinetic Trapping at the One Nanometer Limit. *Proc. Natl. Acad. Sci. U. S. A.* **2011**, *108*, 8937 -8942.

(56)   Wang, Q.; Moerner, W. E. An Adaptive Anti-Brownian Electrokinetic Trap with Real-Time Information on Single-Molecule Diffusivity and Mobility. *ACS Nano* **2011**, *5*, 5792-5799.

(57)   Footnote: Certain commercial equipment, instruments, or materials are identified in this paper in order to specify the experimental procedure adequately. Such identification is not intended to imply recommendation or endorsement by the National Institute of Standards and Technology, nor is it intended to imply that the materials or equipment identified are necessarily the best available for the purpose.

(58)   Berglund, A. J.; Mabuchi, H. Tracking-Fcs: Fluorescence Correlation Spectroscopy of Individual Particles. *Opt. Express* **2005**, *13*, 8069-8082.

(59)   Footnote: The mean-square displacement *within a curved interface* is slightly large than Δr. We neglect this correction, which is of order $(\Delta r/R_{drop})^2 \approx 10^{-3}$ for typical values around $\Delta r \approx 200$ nm and droplet radius $R_{drop} \approx 5$ μm.

(60)   de Juan, E., Jr; McCuen, B.; Tiedeman, J. Intraocular Tamponade and Surface Tension. *Surv. Ophthalmol.* **1985**, *30*, 47-51.

(61)   Berglund, A. J. Statistics of Camera-Based Single-Particle Tracking. *Phys. Rev. E* **2010**, *82*, 011917.

(62)   Michalet, X. Mean Square Displacement Analysis of Single-Particle Trajectories with Localization Error: Brownian Motion in an Isotropic Medium. *Phys. Rev. E* **2010**, *82*, 041914.

(63)   Berglund, A. J.; McHale, K.; Mabuchi, H. Feedback Localization of Freely Diffusing Fluorescent Particles Near the Optical Shot-Noise Limit. *Opt. Lett.* **2007**, *32*, 145–147.

Table of Contents Graphic